Design and performance of a wireless sensor network for catchment-scale snow and soil moisture measurements

Branko Kerkez,[1] Steven D. Glaser,[1] Roger C. Bales,[2] and Matthew W. Meadows[2]

Received 28 July 2011; revised 11 July 2012; accepted 22 July 2012; published 12 September 2012.

[1] A wireless sensor network (WSN) was deployed as part of a water balance instrument cluster across a forested 1 km^2 headwater catchment in the southern Sierra Nevada of California. The network, which integrates readings from over 300 sensors, provides spatially representative measurements of snow depth, solar radiation, relative humidity, soil moisture, and matric potential. The ability of this densely instrumented watershed to capture catchment-scale snow depth and soil moisture distributions is investigated through comparison with three comprehensive gridded surveys and 1 day of detailed lidar snow data. Statistical analysis shows that the network effectively characterized catchment-wide distributions of snow depth, while offering a cost-effective, reliable, and energy-efficient means for collecting distributed data in real time. A temporal analysis of snow depth variability reveals that canopy cover is the major explanatory variable of snow depth and that under-canopy measurements persistently show higher variability compared to those in open terrain. An analysis of soil moisture shows lower variability at deeper soil depth and a correlation between mean soil moisture and variability for shallow soils. A three-phase design procedure was used to optimize the WSN deployment. First, as off-the-shelf performance of current WSN platforms for large-scale, long-term deployments cannot be guaranteed, statistics from a prototype deployment were analyzed. Two indicators of network performance, the packet delivery ratio and received signal strength indicator, showed that for our site conditions, a conservative 50 m node-to-node spacing would ensure low-power, reliable, and robust network communications. Second, results from the prototype were used to refine hardware specifications and to guide the layout of the full 57-node wireless network. Of these nodes, 23 were used actively for sensing, while the remaining 34 nodes were used as signal repeaters to ensure proper spatial radio coverage and robust network operations. Further analysis of network statistics is conducted during the third, operational, phase to validate system performance.

Citation: Kerkez, B., S. D. Glaser, R. C. Bales, and M. W. Meadows (2012), Design and performance of a wireless sensor network for catchment-scale snow and soil moisture measurements, *Water Resour. Res.*, *48*, W09515, doi:10.1029/2011WR011214.

1. Introduction

[2] A comprehensive understanding of the mountain water cycle demands a deeper insight into the spatiotemporal coupling between various hydrologic processes at the headwater catchment and larger-basin scales. This is particularly true in the mixed-conifer zone of California's Sierra Nevada, a productive ecosystem situated in the midelevation rain-snow transition zone, where rain falls at elevations below 1500 m, and snow accumulates above 2200 m [*Bales et al.*, 2006]. It has been noted that this transition zone is sensitive to annual temperature fluctuations, both in terms of the quantities of accumulated snow, as well as melt timing [*Christensen et al.*, 2008]. A complete understanding of the links between snow cover and soil moisture on the forest water cycle is still lacking.

[3] One of the major challenges in hydrologic science relates to characterizing and understanding spatial variability [*Bogena et al.*, 2010]. Spatial measurement of hydrologic processes at the catchment, and basin scales is subject to significant constraints in energy, accessibility, sensor coverage area, and cost. Many off-the-shelf data-logging components do not lend themselves to real time data acquisition when sensors are spatially distributed at the kilometer scale, as wiring runs are limited by prohibitive cost, signal noise and the need to maintain acceptable levels of current. Transmission along wires is further complicated by heavy snow loads, and the proclivity of rodents to chew on cables. Recent advances in sensing technology, particularly in the area of wireless sensor networks (WSNs), now enable environmental monitoring in

[1]Department of Civil and Environmental Engineering, University of California, Berkeley, California, USA.
[2]Sierra Nevada Research Institute, University of California, Merced, California, USA.

Corresponding author: B. Kerkez, Department of Civil and Environmental Engineering, University of California, Berkeley, CA 94720, USA. (bkerkez@berkeley.edu)

0043-1397/12/2011WR011214

real time, and at unprecedented spatial and temporal scales. While access to real time data reduces site visits and inconvenience experienced during scientific research campaigns, a major benefit of distributed real time data relates to decision-making support and operational hydrology. For example, future reservoir operations could be guided more optimally given detailed real time access to spatiotemporal data of upstream water bodies and watersheds. *Rice and Bales* [2010] analyzed the performance of a prototype WSN and concluded that the technology can be effectively used to capture spatially representative measurement of snow depth with relatively few sensors.

[4] For most spatially distributed sensor deployments it is often challenging, and inconvenient, to physically collect cached data, readily detect faulty hardware, and alter equipment parameters. While there are many commercial wireless systems that can transmit data between two points, such hardware generally use relatively high-powered radios and requires substantial energy for transmission. Such point-to-point transmission systems operate independently, and can interfere with each other if multiple links are deployed within a region. WSN technology offers an alternative for cost-effective instrumentation of extended regions with limited accessibility, while permitting real time data access to distributed sensors through a centralized communication architecture. Given the nascent nature of low-power wireless, in particular for remote field applications, off-the-shelf performance cannot be guaranteed, and much work remains to be conducted to quantify the real-world performance of WSNs for hydrologic monitoring.

[5] The research reported in this paper aims to develop techniques for efficient, scalable, and robust WSN deployments for monitoring hydrologic phenomena, while using methods that can readily be extended to many environmental monitoring applications. We address four specific questions: First, what soil moisture and snow depth variability patterns are revealed by strategically distributed sensors in a densely instrumented mountain catchment, and how do these sensor readings compare to gridded surveys and lidar data? Second, what is the performance of a large-scale, low-cost WSN built from off-the-shelf hardware, when exposed to the harsh conditions in the snow covered Sierra Nevada? Third, which metrics can be used to quantify WSN performance and to evaluate the design of the wireless monitoring system? Fourth, what is an efficient approach to designing and deploying WSNs for long-term environmental monitoring campaigns, while maintaining robust and reliable network performance?

2. WSN Design Principles

[6] The core component of a WSN is known as a mote—a tiny, ultralow-power radio operated by a microcontroller and featuring analog and digital interfaces to which sensors can be connected. A mote exchanges information wirelessly with neighboring motes in a distributed network, which can relay this information to their neighbors, until the data reaches a central hub. Software optimization of power control (also known as duty cycling) allows some devices to operate for several years on a pair of AA batteries [*Karl and Willig*, 2005; *Dust Networks*, 2006]; embedded software can be optimized to permit motes to remain in an extremely low-power state the majority of the time (powering the most necessary components, such as the clock and basic microcontroller features), waking up only periodically to transmit or receive data [*Institute of Electric and Electronics Engineers* (*IEEE*), 2009; Dust Networks, Embedded wireless sensor networks for monitoring and control, http://www.dustnetworks.com]. The recent mass adoption of these devices, particularly for industrial applications, has made them an extremely cost-effective alternative to placing wires [*International Society of Automation* (*ISA*), 2009; *Song et al.*, 2008; Emerson Wireless Process Management, http://www2.emersonprocess.com/en-US/plantweb/wireless; Honeywell Industrial Wireless Mesh Solutions, http:/www.honeywell.com/ps/wireless].

[7] Depending on the implementation and protocols of the network stack (the general hardware and software architecture), motes can aggregate into a number of network topologies. The two most common are the star and the mesh topologies (Figure 1). In a star configuration, each mote exchanges information only with a central base station. In the majority of such implementations, the base station is programmed to keep its radio on continuously to listen for incoming transmissions, which results in high energy usage. The span of a star network is limited by the distance of a single link between a mote and its network manager. The network manager is thus often placed in a central location. While it is possible to increase transmission distance using more powerful radios, star networks are still limited by the lack of radio path redundancy and the need to communicate with one central location. If the region being instrumented cannot be covered by a single star network, the ZigBee Protocol specifies a hybrid topology, which enables router nodes to be added to the network to extend coverage [*Bogena et al.*, 2010; ZigBee Alliance, ZigBee specification, http://www.zigbee.org/Standards]. These nodes serve as range extenders, typically using more radio resources to listen for incoming transmissions from nearby nodes, and then forwarding this data to the base station or other nearby router nodes. Given their specialized function, and higher power consumption, most networks use limited router nodes, which limits path redundancy to the base station.

[8] In a mesh-based topology, motes communicate with multiple neighbors to create an internally redundant multihop network. Multiple paths between network nodes allow data to be transmitted even if certain network links fail [*Karl and Willig*, 2005]. Although requiring a relatively larger software overhead, mesh networks can adapt their topology to reflect varying attenuation of radio signals caused by changes in the environment, or changing needs of the operator. The mesh-topology thus allows the network to span much larger areas, compared to a star layout, as out-of-range motes can exchange data by transmitting, or hopping, it via any neighboring motes in the mesh.

[9] Data transmitted within WSNs is quantized into formatted data blocks called packets [*Tanenbaum*, 2003]. A successful transmission is achieved if the transmitting mote receives an acknowledgment from the receiving mote, notifying it that the transmitted data packet has been received correctly. This acknowledgment redundancy, while not built into all available WSN platforms, ensures that packets reach their intended destination, even if retransmission is required.

[10] Since remote wireless networks operate on battery power, overall power consumption becomes a critical constraint. As radio transmissions consume more than 95% of a mote's of power use [*Dust Networks*, 2006] (not including sensors), it is important to design WSNs that will minimize

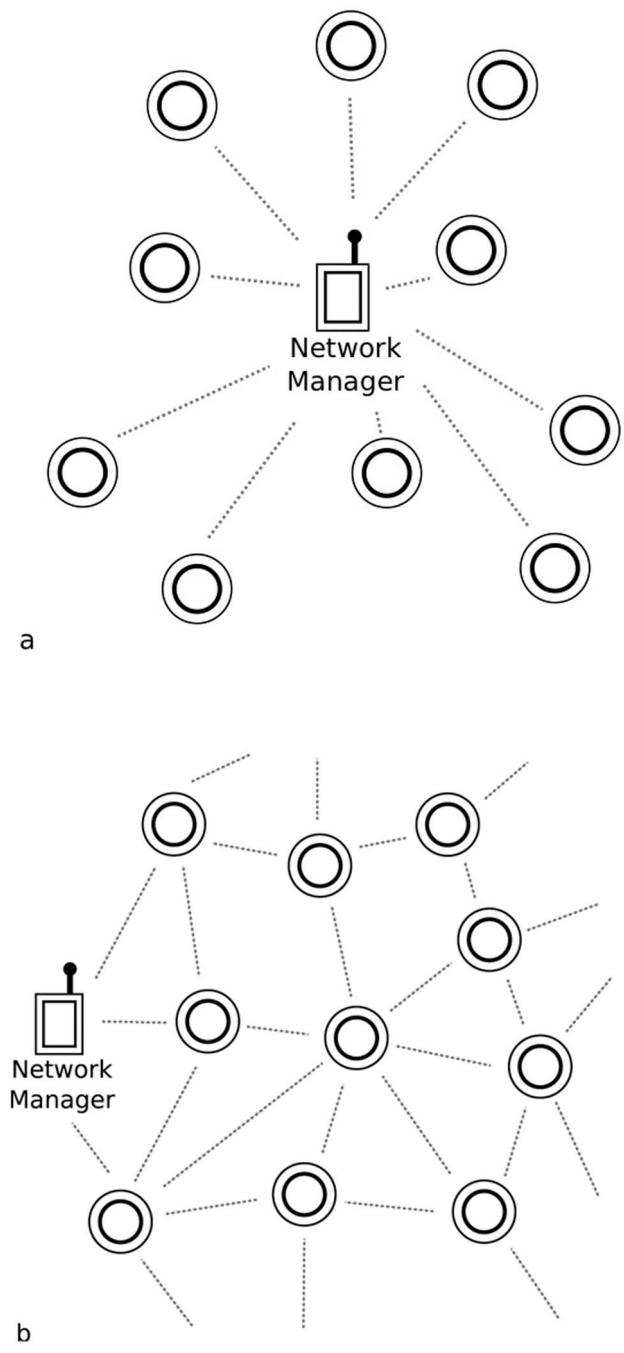

Figure 1. WSN network topologies. (a) WSN star-topology: all motes have a direct link to the network manager; the span of this network is limited by the distance between a mote and the manager. (b) WSN mesh-topology: motes exchange information with neighbors to create a redundant multi-hop network.

retransmissions. By optimizing use of radio resources, and ensuring low power use, motes can be added to an existing data logging infrastructure to provide real time wireless data access, without significantly increasing overall power consumption. Extreme weather conditions, especially cold weather, can take significant tolls on hardware and batteries [*Hasler et al.*, 2008; *Mainwaring et al.*, 2002]. Successful design and operation of such a field-deployed WSN hinges upon a rational set of metrics that can be used to quantify performance.

[11] Communication in WSNs is challenged by multipath radio propagation and narrow-band interference [*Karl and Willig*, 2005; *Watteyne et al.*, 2010] where topography can result in radio signals bouncing off ambient surfaces, causing phase-shifted copies of the same signal to arrive at the receiver antenna. This can lead to destructive interference, which cancels out the original signal, effectively eliminating the ability of certain mote pairs to communicate. The adverse effects of multipath propagation on radio communications are a function of the deployment environment, and it has been shown that even slight changes in node-to-node distance (on the order of centimeters) can have significant impact on this behavior [*Watteyne et al.*, 2009].

[12] The IEEE802.15.4 standard divides the 2.4 GHz band into 16 transmission channels (or, narrow-band subfrequencies) that can be used to mitigate communication challenges posed by external interference and multipath propagation [*IEEE*, 2009]. Improper channel selection can cause data to be lost during transmission, leading to the need to retransmit data, and manifesting itself in much higher energy requirements on the network [*Watteyne et al.*, 2009]. A common approach to address this issue is to conduct an expert survey, which entails a physical visit to the field to select the frequency channel on which the loss of transmitted packets will be minimized. This approach has major drawbacks, as research has shown that the optimal channel may vary over time [*Kerkez et al.*, 2009; *Watteyne et al.*, 2010]. It has been shown that in arboreal environments propagation of radio waves is adversely affected [*Oestges et al.*, 2009], and fluctuations in the surrounding environment can cause poor performance on channels that originally performed well. An option to address this time-varying behavior involves equipping WSNs with the ability to channel hop. In such deployments, motes within the network randomly select one of the available channels every time a transmission occurs, rather than persistently transmitting information on a single channel. While still an area of ongoing research [*Kerkez et al.*, 2009; *Watteyne et al.*, 2010] and requiring slightly larger implementation overhead, channel hopping has been shown to reduce the effects of multipath propagation and external interference, thus improving network reliability and battery lifetime.

[13] A number of commercial WSN solutions are available (Dust Networks, http://www.dustnetworks.com; Ember, ZigBee wireless network systems, http://www.ember.com/; Jennic Wireless Microcontrollers, http://www.jennic.com; Libelium, Wireless sensor networks, http://www.libelium.com; Nevis, Persistent LAN security and network access control, http://www.nevisnetworks.com; Sentilla, Enterprise management for energy, http://www.sentilla.com), each offering distinct platforms with unique functionality, network stacks, and standards. The implementation of algorithms for network topology, routing, and channel hopping is a nontrivial task, but advances in WSN technology have alleviated, although not completely removed, many of these challenges. No simple off-the-shelf solution exists for environmental monitoring applications, and hardware performance can vary significantly depending on site conditions.

[14] Deployments of WSNs have ranged from data center HVAC control [*Bell and Federspiel*, 2009] structural health monitoring [*Kim et al.*, 2007; *Rice and Spencer*, 2008], and military applications [*Culler et al.*, 2001]. Notable deployments for environmental monitoring purposes include habitat

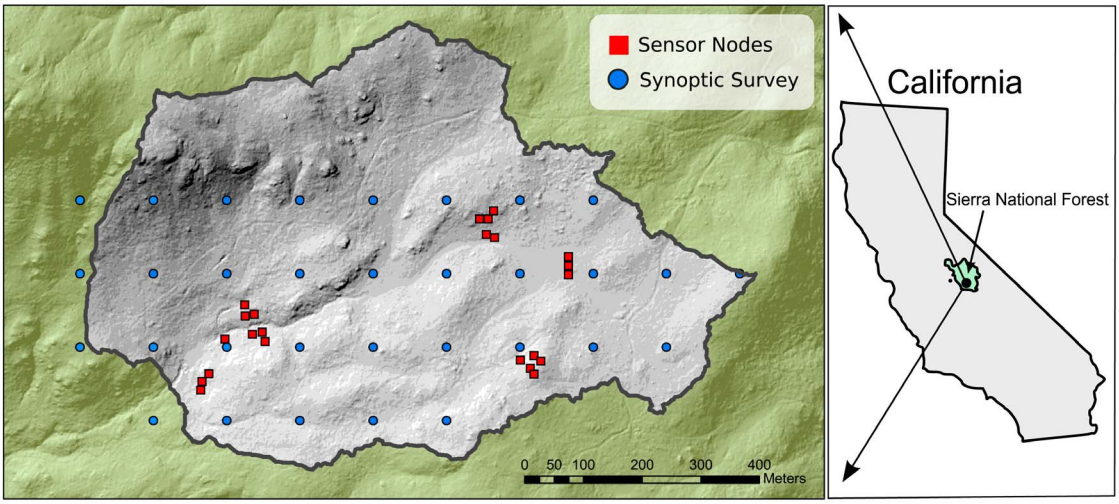

Figure 2. Site location (37°04′N, 119°11′W) showing location of sensor nodes and synoptic survey sampling points.

monitoring [*Hart and Martinez*, 2006; *Mainwaring et al.*, 2002; *Ramanathan et al.*, 2006], permafrost detection [*Hasler et al.*, 2008], the study of mountain ranges [*Ingelrest et al.*, 2010], and for purposes of snow depth monitoring [*Rice and Bales*, 2010]. A successful short-term deployment of a WSN for the monitoring of hydrologic phenomena was conducted by *Trubilowicz et al.* [2009], who noted that the technology they tested lacked ease of use and reliability. Further examples of wireless deployments for ecological and environmental monitoring were conducted by *Etzel and Braun* [2005], *Porter et al.* [2005], and *Szewczyk et al.* [2004]. Most recently, the efficacy of a large ZigBee-based network for monitoring soil moisture variability was also verified by *Bogena et al.* [2010]. The hardware and software implementations in these studies varied significantly, making it difficult to gauge which hardware, software, and network protocol implementation will perform the best for a given deployment. The current lack of the out-of-the-box usability, coupled with the vast choice of available hardware and network protocols, has the potential to become a severe time drain for scientists designing an environmental monitoring system.

3. Methods

3.1. Network Design

[15] Twenty-three locations were selected and instrumented to monitor water balance variables in a remote, forested, headwater catchment along a 1.5 km transect in the Southern Sierra Critical Zone Observatory (CZO) (37°4′ N, 119°11′ W), which is colocated with the Kings River Experimental Watershed (KREW) [*Bales et al.*, 2011; *Levia et al.*, 2011]. KREW spans the rain-snow transition zone, with lower elevations receiving more precipitation as rain. The WSN is located in a northern, relatively higher elevation subcatchment of KREW, where the majority of annual precipitation falls as snow. Site elevations in the WSN-instrumented catchment range from 1950 to 2010 m, with landscape varying over dense mixed-conifer forest (76–99%), open meadows, and across mixed chaparral, and barren land cover.

[16] In the summer of 2009, sensors were placed at those 23 locations prior to WSN design (Figure 2). The locations were selected in the field to reflect variability in catchment-wide physiographic parameters, such as aspect, elevation, and canopy cover. Particular focus was given to previous studies [*Faria et al.*, 2000; *Molotch and Bales*, 2005; *Musselman et al.*, 2008; *Rice and Bales*, 2010], which identified these major physiographic parameters as driving explanatory variables for snow depth. Each location was instrumented with snow depth, solar radiation, and relative humidity sensors (Table 1). One meter deep soil pits were excavated at each location and the face of each pit was instrumented with soil moisture and matric potential sensors at 10, 30, 60, and 90 cm depths, unless physically prohibited by bedrock. The soil moisture sensors were installed in undisturbed soil, and the matric potential sensors were installed in nearby disturbed soil at the same depth. The soil profiles were then backfilled and hand compacted to maintain the original soil horizons and density as much as possible (see *Bales et al.* [2011] for more detail and volumetric water content calibration procedure). A Judd snow depth sensor was also mounted 3 m above ground surface on a 75 cm cantilever beam.

[17] Along with two additional temperature measurements, this provided over 15 sensors readings at each measurement node (Figure 3), giving a total of over 300 sensors for the entire network. Our deployment makes a distinction between sensor nodes, which are motes interfaced with the

Table 1. Sensor Characteristics

Parameter	Sensor	Manufacturer	Accuracy
Snow depth	Ultrasonic	Judd Communications	±1 cm
Volumetric water content	EC-TM	Decagon	±3% VWC
Matric potential	MPS-1	Decagon	Calibration dependent (maximum ±40%)
Solar radiation	LI-200	LI-COR	±5%
Humidity and temperature	SHT15	Sensirion	±2%, ±0.5°C

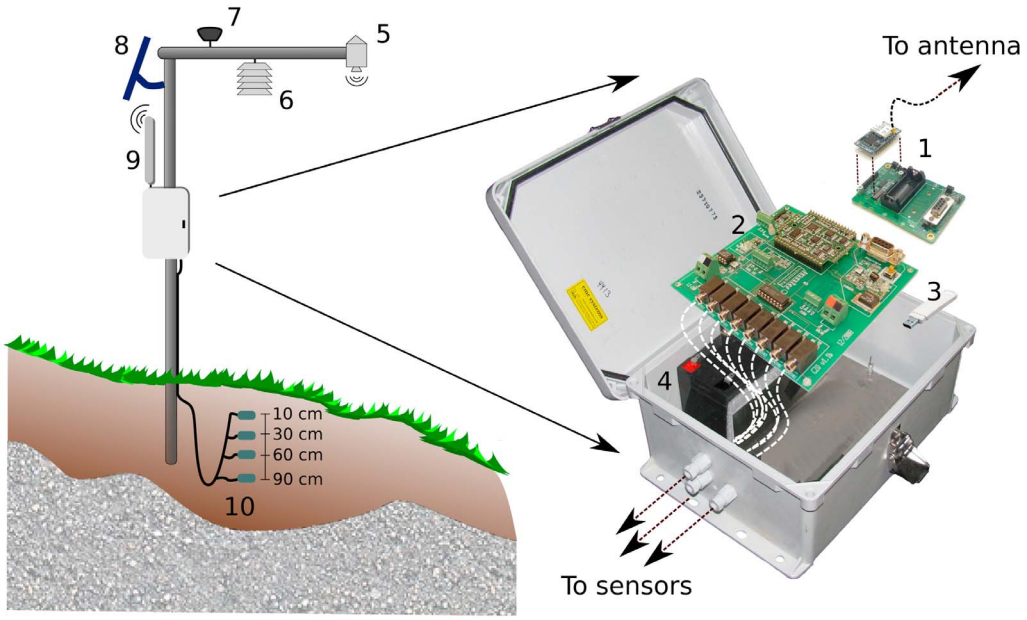

Figure 3. Sensor node architecture. (1) Mote, (2) custom data-logger to interface the sensor array, (3) on-site memory storage, (4) 12V battery, (5) snow depth sensor, (6) humidity and temperature sensor, (7) solar radiation sensor, (8) 10W solar panel, (9) external 8dBi antenna, (10) four soil moisture, temperature, and matric potential sensors at varying depths.

sensors and data-logging infrastructure (Figure 3), and repeater nodes, which only contain motes and a power source, placed to ensure mesh redundancy, and to transfer data between locations which would otherwise be out of range.

[18] The WSN deployment was carried out in two steps. A smaller-scale prototype deployment was conducted in September 2009, relying on manufacturer-specified transmission distances as guide to mote placement (Figure 4). This network was mainly composed of sensor nodes (red points in Figure 2) and a few repeater nodes. Site-specific network statistics were collected to evaluate the performance of the WSN prototype. An analysis of these statistics, using a set of WSN metrics, was then used to inform a network-wide redesign. Further repeater nodes were then added to the network, and existing repeater nodes were relocated to ensure desirable network performance, establishing the final network configuration of 57 WSN nodes.

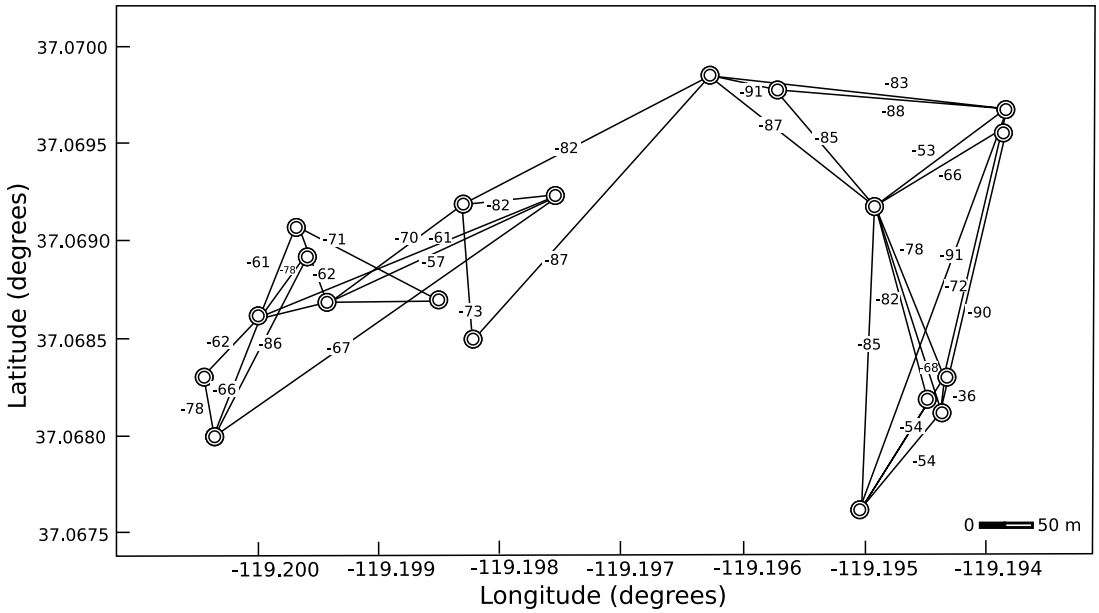

Figure 4. Snapshot of the prototype network. Circles indicate locations of motes. The figure lists path-specific RSSI values in dBm (decibels referenced to 1 mW).

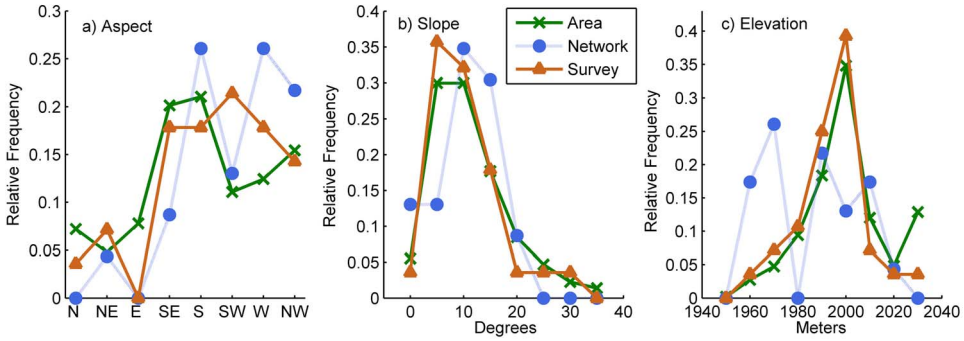

Figure 5. Comparison of physiographic parameters captured by LIDAR, against those covered by the sensor-nodes, and synoptic survey.

3.2. Synoptic Surveys and Variability Analysis

[19] To evaluate the ability of the WSN to capture catchment-scale hydrologic variability, data from gridded synoptic surveys were used to provide ground truth for the distribution of soil moisture and snow depth. The surveys were carried out in the larger CZO, but this analysis will only focus on the measurements specific to the subcatchment instrumented by the WSN. The survey grid points were selected to evenly cover 125 m intervals (Figure 2). The points were located in the field using a Magellan handheld GPS unit with 3–5 m accuracy. A snow depth survey was carried out on 7–9 April 2010. At each point, three depth measurements were taken 5 m apart in a N-S transect using a snow depth probe. When possible, each of the three measurements was taken under varying canopy cover (under canopy, canopy drip edge, and open terrain). Two soil moisture surveys were also conducted on 14–17 June and 6–10 September 2010 using a handheld Hydrosense soil moisture system. Five synoptic measurements were taken within a 30 × 30 cm area and average values were used. Synoptic measurements were integrated over the top 20 cm of soil. These readings were compared to the average of the 10 cm and 30 cm readings taken by the Decagon soil moisture probes in the network. Prior to the survey, the Hydrosense system was calibrated to soil obtained from the site, and compared to the Decagon soil moisture probes. It was determined that no significant difference in the measurement methods was apparent. In few cases, field conditions and accessibility did not permit some survey points to be sampled.

[20] Lidar data sets with 1 m^2 resolution were also collected both for snow-on and snow-off conditions [*Guo et al.*, 2010]. The snow-on lidar data set was collected on 22–23 March 2010, and the total snow cover was calculated by subtracting the snow-off raster from the snow-on raster in the ArcGIS software package. To assess the ability of the lidar data set to capture catchment-wide snow depth distribution, and to validate the use of the lidar data for purposes of this study, a comprehensive ground truth survey was conducted on the day of the snow-on lidar flight. Manual snow depth readings, spaced 10 m apart in a cross-shaped transect, were taken at forty locations in a central part of the catchment and tagged via handheld GPS units during the snow-on lidar survey. Along with the snow depth readings taken at the sensor nodes, these points revealed an average error of less than 10 cm when comparing lidar-derived snow depth data to ground truth readings. Furthermore, the snow-off lidar raster was used to delineate the catchment instrumented by the WSN using the Spatial Analyst toolbox in ArcGIS. The resulting delineation is shown in Figure 2 as a shaded relief map.

[21] An analysis was also carried out to investigate the temporal trends in snow depth and soil moisture variability. The results were compared to previous studies, which evaluated forest canopy effects on snow depth variability [*Jost et al.*, 2007], the effects of soil depth on volumetric water content (VWC) variability (as measured by the coefficient of variation (CV)) [*Famiglietti et al.*, 1998; *Grant et al.*, 2004], as well as the dependence of VWC variability on mean VWC [*Bogena et al.*, 2010; *Famiglietti et al.*, 1998; *Grant et al.*, 2004; *Vereecken et al.*, *2007*; *Wackerly et al.*, 2008]. A geostatistical analysis was also performed on the snow depth and soil moisture data sets [*Bogena et al.*, 2010; *Western et al.*, 2002; *Deems et al.*, 2006] to evaluate effects of spatial scaling on sampling design.

[22] The distribution of aspect and slope captured by the network and synoptic surveys reflected those of the more comprehensive lidar survey (Figure 5), but the network did not capture some of the higher elevations (1990–2040 m) located in the northern portion of the catchment (Figure 2). These locations were excluded from the sensor placement in favor of sampling nearer the stream. The sensor nodes were also positioned under various canopy covers, with 30% of nodes under canopy (UC), 30% in open terrain, and 40% at tree drip edge (DE).

3.3. Hardware

[23] The fluctuating humidity, heavy storms, and cold winter temperatures at the site called for special considerations during the design of the monitoring hardware. Reliability requirements demanded specific attention to the underlying network control algorithms, as well as the selection of the appropriate transmission frequencies. The system uses wireless devices developed by Dust Networks (http://www.dustnetworks.com/), a company that primarily develops wireless data transfer technologies for industrial automation applications. The hardware, in our case the M2135 mote, is rigorously tested at extreme environmental exposures to meet stringent industrial guidelines, motivating its use in the harsh conditions of the Sierra Nevada. The core software backbone of the Dust WSN relies on the Time Synchronized Mesh Protocol (TSMP) architecture [*Dust Networks*, 2006; *Pister and Doherty*, 2008], which closely follows a number of well-specified industrial wireless protocols [*ISA*, 2009; *Song et al.*, 2008]. An open source version of TSMP is also

Table 2. Power Consumption of Various Components in the Network Assuming a 15 min Sampling Interval

Component	Voltage (V)	Current (Idle) (A)	Duty Cycle (%)	Average Current (A)
Mote	3	0.02 ($<2 \times 10^{-5}$)	<1	6×10^{-6}
Data logger	12	0.02 (2×10^{-4})	1	4×10^{-4}
Sensors	5–12	0.1	1	1×10^{-3}
Network manager	12	0.06	100	0.06
Cellular modem	12	0.4 (<0.1)	50	0.2
Embedded computer	5	0.3	100	0.3

available for implementation on most hardware platforms [*Watteyne et al.*, 2012].

[24] These industrial protocols are built upon three main principles: time synchronization, channel hopping, and automated multihop smart mesh formation. Motes within a TSMP network are synchronized to within submillisecond accuracy. This enables accurate time stamping of sensor data, and permits motes to keep their radios off more than 99% of the time by only communicating according to a dynamically determined scheduled. While such tight time synchronization facilitates an extremely low radio duty cycle, and thus significantly lowers battery usage, it also permits for channel hopping. Along with scheduling transmissions, motes in a TSMP network account for fluctuations in the radio space by scheduling a different frequency channel for each transmission. This approach effectively utilizes all 16 available channels defined by IEEE802.15.4 [*IEEE*, 2009]. This mitigates the previously mentioned effects of multipath fading and external radio interference by ensuring that no two mote pairs communicate on the same channel at the same time. This significantly differs from ZigBee based networks (ZigBee Alliance, http://www.zigbee.org/Standards), where one frequency channel is often used for the entire network, and limited synchronization can lead to intranetwork radio interference due to lack of an explicit transmission schedule. The TSMP protocol also features dynamic smart-meshing algorithms, which allow each mote to automatically join the network, and adaptively communicate with multiple neighbors, without the need for specialized router nodes seen in ZigBee networks. The adaptive nature of this WSN also changes network paths (links, or node-to-node routes) dynamically to reflect possible network interference from outside sources, or changing field conditions. The availability of the TSMP features, all of which, to our best knowledge, are not implemented on other commercial platforms, motivated the decision to use Dust Networks hardware for this deployment. Each mote is powered by a 3 V battery and has a manufacturer-specified battery life of over 2 years.

[25] The WSN featured one base station, or network manager, that acted as a central network controller. The network manager communicated with a low-power, embedded Linux computer via Ethernet and the two devices exchanged commands over an extended markup language (XML) interface to actuate motes within the network, log sensor readings, and gather network statistics. The embedded computer was located at the base of a 50 m tower used for eddy correlation. A cellular modem positioned 25 m up the tower provided Internet connection for the transfer of real time data to an off-site location. Power to the network manager, embedded Linux computer, and cellular modem was provided by a bank of 12 V batteries and a 120 W solar panel. Careful selection of low-power components enabled battery-powered operation of the base station without the need for outlet power.

[26] Anomaly detection within the network was conducted by custom software that was written to interact continuously with the network manager to monitor network statistics and sensor readings, informing network operators of impending battery outages, sensor failures, or other events of interest. To further improve transmission distance, physically hardened, high-gain 8 dBi antennas were mounted 3 m above ground surface at each network node.

[27] While commonly used data logging components, such as the Campbell Scientific CR1000 line (Campbell Scientific, http://www.campbellsci.com/cr1000), could be interfaced with the wireless hardware, a more cost effective, and more customizable data-logging board was designed to control and power the sensor array, as well as to form the data into serial packets required for transmission by the Dust Networks mote. The board is the EME Systems OWL2pe data logger (Electronically monitored ecosystems, http://www.emesystems.com/), and interfaces nine analog and twenty digital inputs, allowing for additional sensors to be attached in the future. The board requires about 240 mW of power while actuating sensors, but spends 99% of its time in an efficient low-power mode. The OWL2pe can be self-contained, or controlled remotely via the WSN, and built in flash memory allows the assembly to log data locally in case the WSN becomes unresponsive. Lack of accessibility to the physical network, especially during heavy snow periods, as well as the possibility of long-lasting diminution of solar radiation, played a significant role in the design of the power management infrastructure. Monitoring requirements called for data to be collected on 10–15 min intervals, and conservative preliminary calculations indicated that a 12 volt, 7 amp-hour lead-acid battery, and a 10 W solar panel, could reliably power the data logger and sensor assembly. To mitigate the effects of extremely cold temperatures, the repeater nodes were equipped with 3.6 V lithium thionyl chloride batteries. The power consumption of network components is shown in Table 2.

3.4. System Cost

[28] At the time of deployment the cost of each mote was under US$50, with an additional $500 for a sensor node, including custom data logger, housing, mounting, and external antenna. Base station components, including the network manager, Linux computer, cellular modem, enclosure, batteries and solar panel totaled about $3000. Sensors used in the study comprised the biggest cost, varying in price from $25 to $600 each, the most expensive of which was the snow depth sensor.

3.5. WSN Metrics

[29] The packet delivery ratio (PDR), and received signal strength indicator (RSSI) are two metrics that provide particular insight when evaluating WSN performance [*Al Basset Almamou et al.*, 2009; *Karl and Willig*, 2005]. PDR is a metric that captures the overall communication efficiency of a link between two WSN nodes, and is defined as the number of successfully transmitted packets divided by the total number of transmitted packets. It can be thought of as the probability that a transmission between two nodes will succeed. Needless retransmission of a packet can take a

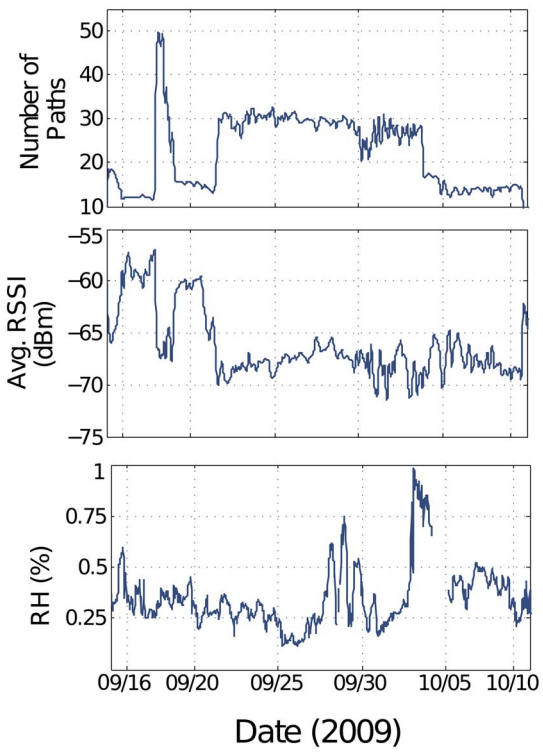

Figure 6. Network behavior over a 25-day period, starting on September 15, 2009. Network resets are evident as the sudden spikes in number of network paths. The average RSSI of nodes in the network dropped as more paths were created (more nodes joined the network). A rainstorm, evident around October 3, coincided with a significant drop of paths from the network.

significant toll on battery resources. Conservation of network resources ideally demands a PDR of 100% on all links used by the network. An understanding of the interplay between spatial network coverage and deployment-specific PDR characteristics is thus required. Since a primary motivation of using WSN hardware for environmental monitoring is the ability to span large areas, optimization of a field deployment demands a balance between the need to maximize battery life (power cost) while minimizing the number of required motes (capital and operational costs).

[30] RSSI, conventionally measured in decibels and referenced to 1 mW (dBm), represents the power in a signal when it arrives at the receiving antenna. As a general rule, the RSSI decreases as the distance between two nodes increases (inversely to the square of the distance between two nodes). Given the logarithmic scale, every 3 dBm decrease reduces the received power by approximately one half, and more negative dBm values correspond with lower signal strength. The true behavior of RSSI over node-to-node distance depends upon a number of factors, such as multipath radio propagation and environmental obstructions but can be roughly captured by an idealized Friis antenna propagation model [*Friis*, 1946, 1971; *Kraus*, 1988]. Since this theoretical propagation model is valid only in free space, and does not take into account the effect of multipath radio propagation, the model cannot, in most cases, be used to accurately predict the behavior of most real world phenomena. Generally, WSN hardware has a manufacturer-predefined RSSI threshold (sometimes also referred to as receiver sensitivity) below which signals cannot be reliably decoded by the hardware. Changes in the physical environment affect the received signal strength, thus causing RSSI to fluctuate over time. The operational RSSI threshold (one that gives reliable performance in the field) can often exceed, or underperform, manufacturer specifications, thus placing the onus of classifying link reliability onto the WSN operator. Since RSSI threshold is often used to specify reliable transmission distances, optimizing network performance becomes the job of the network operator (researcher) and depends on understanding the link-specific RSSI behavior for any given deployment. Improper determination of these thresholds can lead to network collapse and the need for reconfiguration during the actual deployment.

[31] Motes have the ability to enter any number of possible sleep states [*Karl and Willig*, 2005; *IEEE*, 2009], where significant portions of the mote are shut off to conserve energy. For example, when a mote is not transmitting or receiving data, it turns off its radio while placing the microprocessor into a low-power state. This significantly reduces power consumption on the battery. A particular problem resulting from an extended lack of communication occurs when motes enter a deep-sleep, or hibernation, state. In such cases, motes that have not been able to establish communications with the network manager through their neighboring motes for a period of time, power off the majority of resources, and wake up only sporadically to rejoin the network by listening to advertising beacons from neighbors. This feature, although not standard on all platforms, was designed to conserve power in industrial mesh networks. When implemented, field experience has shown that it can take significant portions of time (hours to days) for motes to rejoin the network upon entering the deep sleep state. In relatively low node density networks, such as those used for environmental monitoring applications, a mote in a deep sleep state is effectively removed from the network, which has the potential to severely compromise the mesh topology, and can lead to outages of entire subsets of the network. This behavior further underscores the need to understand path specific PDR and RSSI characteristics for ensuring network robustness, and avoiding network outages due to drops in connectivity.

4. Results

4.1. Prototype Deployment

[32] During on-site evaluation of the motes it became apparent that the initial prototype network layout (Figure 4) did not perform up to manufacturer-provided specifications. The specifications indicated an RSSI threshold of −89 dBm, with a prescribed mote-to-mote spacing of up to 200–300 m. In practice, few reliable paths at such distances were observed, and RSSI values between −80 and −90 dBm were experienced for significantly shorter network links. Network statistics were collected over a 25 day period, beginning with 10 motes on 15 September 2009 and expanding to 19 motes by 18 September (Figure 4). RSSI and PDR value were averaged over 15 min intervals for each path in the network, providing a range of values to determine proper hardware thresholds and evaluate network performance. Over this 25 day period, the number of paths (or links between nodes) varied as the WSN automatically adjusted the network topology to account for fluctuations in communication reliability

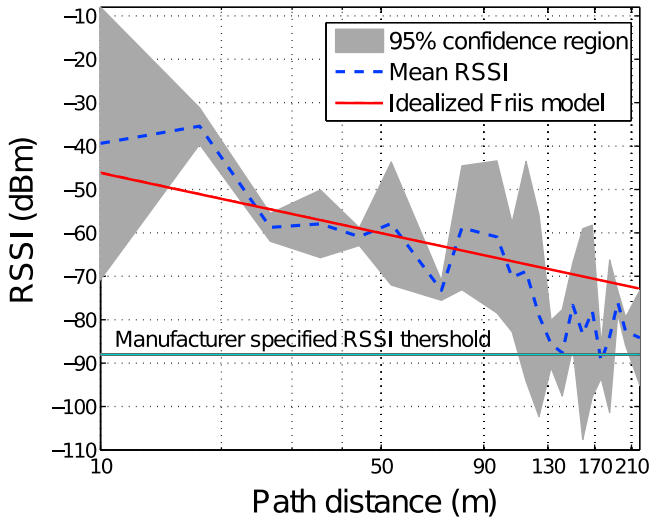

Figure 7. Plot of RSSI vs. path distance collected over a 25 day period. The RSSI decreased with an increase in path distance, and significantly fluctuated around the mean. A number of in situ radio links experienced RSSI values below the manufacturer-specified −89 dBm threshold at approximately 100–120 m.

(Figure 6). Generally, a larger number of paths are desirable since it permits for greater diversity of routes on which data packets can be transmitted. The spike around 18 September corresponds to the deployment of the full 19-sensor prototype network. As more motes joined the network, the number of paths increased correspondingly. The average network RSSI dropped as a result, implying that the newly formed network paths possessed low connectivity. This correlation was observed for the remainder of the 25 day evaluation of the network prototype. Ideal performance would have kept average RSSI steady, regardless of the number of newly created network paths, indicating that all paths reflect similar communication reliability. Further investigation into possible causes of network behavior showed that both the average network-wide RSSI and the average relative humidity experienced fluctuations over time, but did not appear to be positively correlated (Figure 6).

[33] The western portion of the prototype network experienced a complete outage on 19 September, leaving only a few network paths operational (Figures 4 and 6); no prior indication of an impending network outage was evident. During the outage, the total number of paths in the network dropped significantly and abruptly. This can be attributed to a bottleneck effect within the network. In a meshed topology, child nodes far from the network manager need to transmit data through neighboring parent nodes (nodes closer to the network manager), which in turn pass the data further along the mesh until it reaches the network manager. On 19 September critical parent nodes in the mesh drifted into a hibernation state due to a drop in connectivity (most likely due to low RSSI values exhibited by network paths in the center of Figure 4), and child nodes that depended on these connections lost connectivity to the network manager. Child nodes in the western portion of the network were thus forced to enter a hibernation state as well. To avoid this bottleneck phenomenon, redundancy and robustness needed to be built into the network to ensure that no single outages can cause the remainder of the network to fail. This bottlenecking behavior further explains why average network RSSI was inversely proportional to the number of paths. Following this outage, only stable links with high RSSI values remained in the network.

[34] The mote hibernation state was designed to conserve power during network communication outages, since transmission during such instances of low connectivity can significantly shorten battery life. Once in the hibernation state, it could take days for the mote to rejoin the network depending on field conditions, and a physical reset was required to bring motes out of hibernation, and to reestablish the entire WSN mesh. Once the network hardware was reset a week into the prototype deployment, the number of network paths increased and stayed constant for the following 2 week period.

[35] Relative humidity did not seem to affect the overall behavior of the network (Figure 6), but a rainstorm around 3 October 2009 coincided with another network collapse and a significant drop of nodes from the network. To mitigate future network collapse, the TSMP protocol settings could be modified to lower the threshold for entering the hibernation state, or additional repeater motes could be added to ensure that required RSSI thresholds would be met. It was deemed that the low-power sleep mode was necessary for efficient network operations, and that a redesigned network layout would offer a better alternative. This was again confirmed when noticing a significant drain on mote battery life after forced resets.

[36] Part of the predeployment site analysis involved determining the field RSSI as a function of node-to-node distance. Figure 7 presents a logarithmic plot of RSSI versus path distance for the prototype deployment, and for comparison, the idealized Friis propagation model [*Friis*, 1946], which governs how the hardware-specific RSSI between two nodes should change assuming perfectly isotropic antenna and free space conditions. The measured relationship was not monotonic, nor sharply delineated, and showed considerable uncertainty, which was most likely a function of

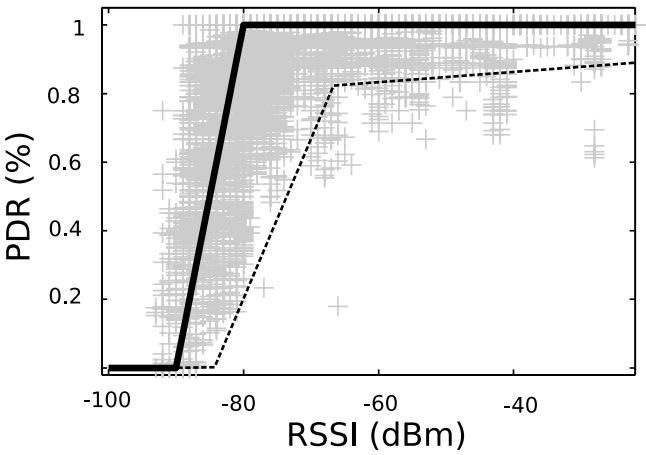

Figure 8. A plot of PDR as a function of RSSI. Gray points reflect observed behavior, while the solid black line represents an idealized waterfall fit. Most packets are transmitted successfully for an RSSI above −80 dBm, after which there is a sudden drop in PDR. The dashed line provides a conservative, and lower bound design curve.

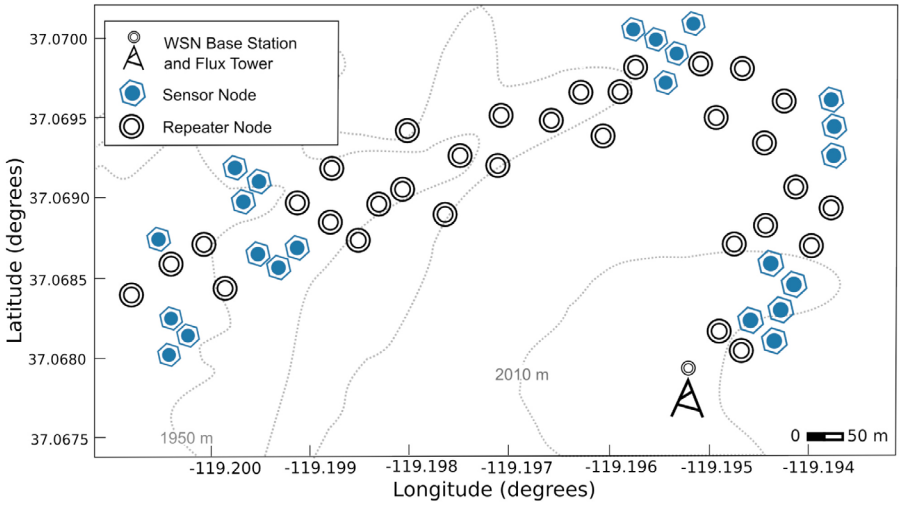

Figure 9. Final wireless sensor network layout. The base station, located at an eddy flux tower, houses a network manager and acts as a central data aggregation point.

multipath effects on radio propagation. The in situ network statistics showed a significant reduction in transmission distance compared to the manufacturer-specified 200–300 m outdoor range. As expected, the observed average RSSI decreased as the distance between nodes increased, but a significant spread existed around the mean (shown by an estimate of the 95% confidence bounds). The mean RSSI reached the manufacturer specified threshold of −89 dBm at a transmission distance of 150 m, but a portion of paths performed below this threshold at the same distance. At 115–120 m separation, a portion of network paths had the tendency to drop below this threshold, underperforming manufacturer specifications of a 200 m range. For distances below 25 m, the network links outperformed the predictions made by the Friis propagation model but mean RSSI significantly deviated from the idealized Friis model after the 25 m mark.

[37] Figure 8 presents another, and perhaps better, indicator of network performance: an analysis of PDR (%) as a function of RSSI (dBm). Although fluctuations of PDR around specific RSSI values existed, it is evident that for values of RSSI over −80 dBm, the PDR remained around 100%, implying high reliability and that few, or no retransmissions were required to successfully deliver network packets to their destination. For values below this RSSI threshold, paths experienced sudden drops of PDR, falling entirely to 0% for RSSI values of −90 dBm and lower. This sudden drop is often referred to as waterfall behavior when describing to the effect of RSSI on PDR.

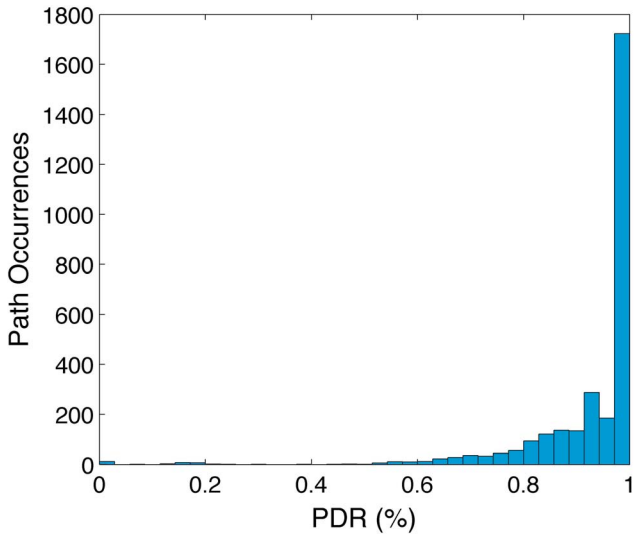

Figure 10. A histogram of PDR values for all paths in the network following a reconfiguration of the network. About 80% of all network paths are performing within the desired 85–90% design value, and over 50% of all paths are at 100% PDR.

4.2. Postdeployment Analysis

[38] Following the prototype deployment, an analysis of network metrics was used to inform a redesign. More repeater

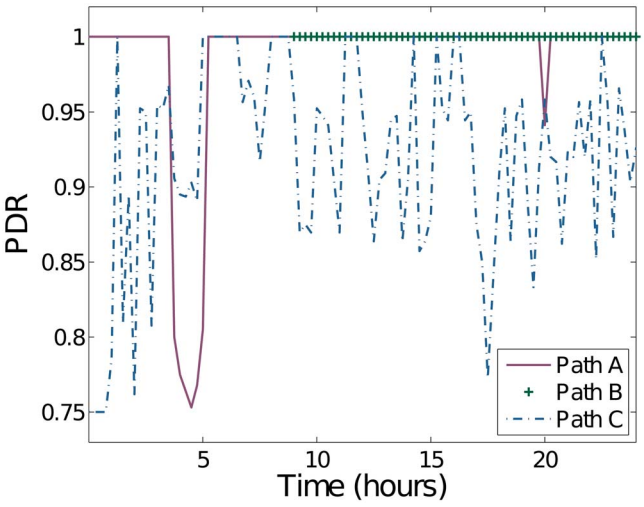

Figure 11. The fluctuations of PDR over time for three specific paths in the network over a 24-hour period.

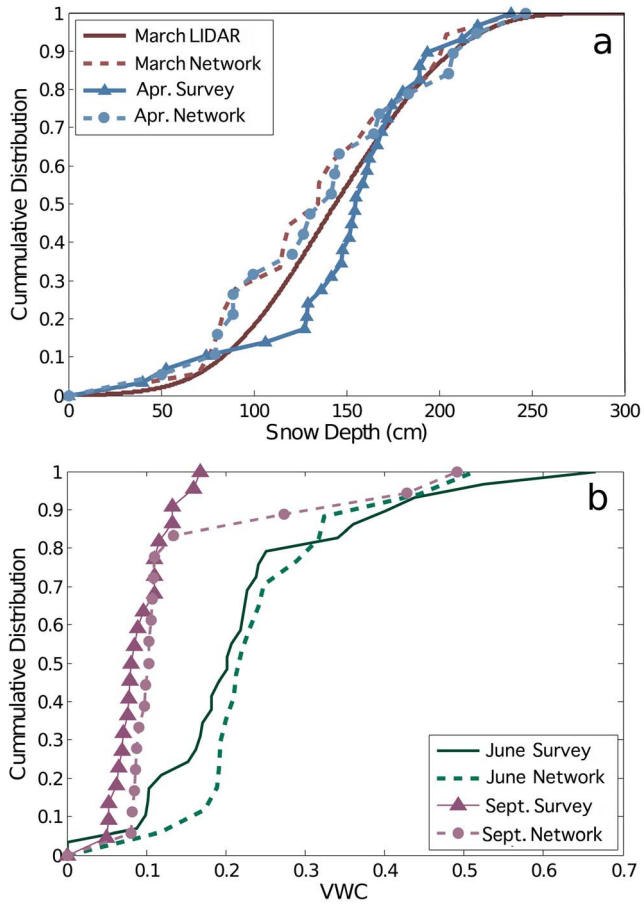

Figure 12. Cumulative distribution functions comparing network readings of a) snow depth, and b) soli moisture to those obtained by synoptic and LIDAR surveys.

nodes were added to the network, and existing repeater nodes were relocated to improve performance and prevent network outages, leading to the final network configuration shown in Figure 9. After redesign, the network did not experience any more outages. A histogram of 30 days of PDR values for all paths in the network (Figure 10) a month after network reconfiguration, shows that about 80% of total PDR values were within a desirable 85–90% performance range, with more than half of all paths experiencing 100% PDR (particularly nodes spaced less than 50 m apart). Nodes communicated not only with their closest neighbors, but also with more distant nodes to maintain the mesh network topology. In the final deployment, network nodes had, at all times, a stable connection to at least two neighbors located 50 m or closer, and the average network-wide PDR remained within an 85–95% window for the remainder of the network lifetime.

[39] To illustrate more some short-term dynamics of the network, Figure 11 shows a sample of PDR evolution for three randomly selected paths in the final network configuration. Though average network PDR remained high, path *A* exhibited a sudden drop at the 4 h mark, only to recover within 1 h. Path *B* exhibited fluctuations of PDR for the entire sample period. While requiring multiple retransmissions of the packets, this path did not drop from the network and its PDR never dropped below 80%. Figure 11 also shows a new network path *C* being established during this 24 h window, which is a positive indication that the self-healing network algorithms dynamically allocated paths to take advantage of more stable connections, thus alleviating otherwise relatively less stable connections and creating further redundancy. The formation of new paths between nodes was caused by fluctuation in the radio space, and is further motivation for using an adaptive, self-healing network.

[40] During network operation, there were some instances of paths longer than 200 m experiencing RSSI values greater than −60 dBm, while some paths less than 50 m operated with RSSI values of −80 dBm. This behavior was not

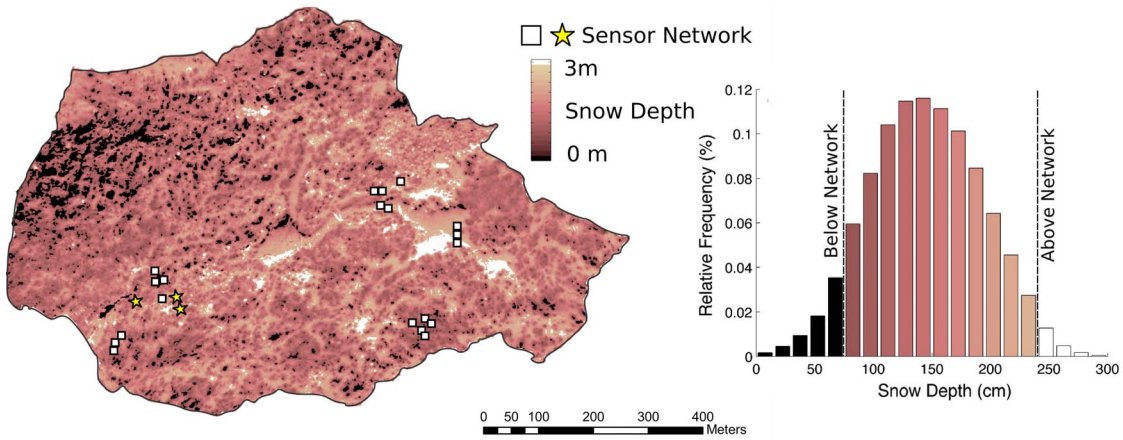

Figure 13. Total snow cover calculated from a snow-off and snow-on LIDAR data sets at 1m2 resolution (March 22–23, 2010). White squares indicate location of sensor nodes. The yellow stars indicate locations of the three sensor-nodes that persistently recorded snow depth values closest to the mean of both the LIDAR-, and synoptic-survey. Histogram of snow depth values calculated from LIDAR data is also shown. Partitioned regions indicate low, and high values not captured within the range the WSN measurements.

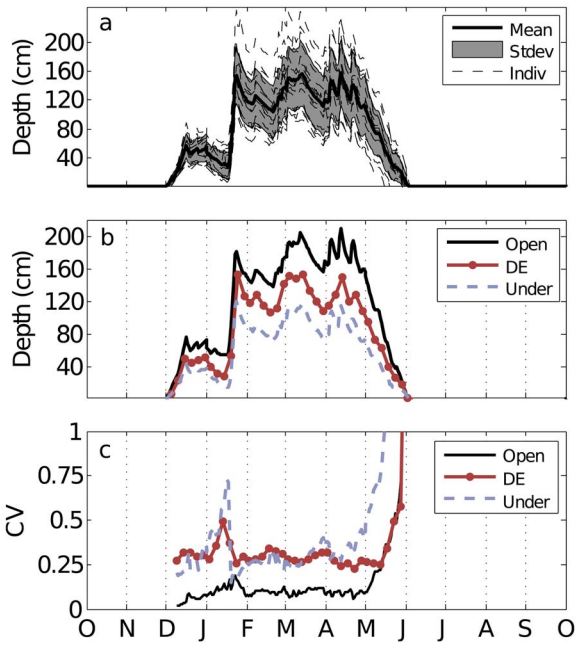

Figure 14. Temporal snowdepth trends October 2009 to October 2010. a) Average snow depth (one standard deviation shown in in gray, individual sensors indicated by dashed lines), b) average snow depth for various canopy covers (open, drip edge, and under canopy), c) Coefficient of variation over time for snow depth and various canopy covers.

consistent across the network, and could not be directly attributed to physiographic features of terrain (such as elevation differences, or line of sight), thus further underscoring the unpredictability of the wireless environment.

4.3. Network Measurement Validation

[41] The mean snow depth measured by the network on 22–23 March 2010 was 139 cm, versus a 145 cm mean from the lidar data (Figure 12a). On 7 April 2010, the network measured a mean snow depth of 142 cm versus 140 cm for the synoptic survey. Although the network and lidar data showed a similar cumulative distribution for 22 March, the network measurements of snow depths varied between 70 and 242 cm, while the lidar snow depths varied between 0 and 300 cm. The cumulative distributions of snow depth for the March lidar, March network and April networks shared a similar, near-normal shape, while the cumulative distribution of the 7 April survey was biased toward relatively high depth values.

[42] For the June soil moisture study, the network VWC measured a mean of 0.23 (standard deviation 0.14), and synoptic survey measured 0.25 (standard deviation 0.09). The cumulative distributions in Figure 12b show the close resemblance between VWC values recorded during the June survey and the June Network measurements. For September 2010, the network reported a mean VWC of 0.15 (standard deviation 0.12), compared to the 0.09 (standard deviation 0.03) in the synoptic survey (Figure 12b). Three network readings, in particular, showed relatively high VWC during the September survey. The respective cumulative distribution of VWC showed a close correspondence between the September survey and network reading up until the inclusion of those relatively higher VWC values captured by the network. These three specific sensor nodes were located in flat-aspect terrain, in open meadows.

[43] A histogram of snow depth distribution, based on the 22 March lidar point cloud, shows that snow depth was near-normally distributed (Figure 13). This distribution was obtained after removing a small set of outliers (<0.1%); i.e., negative values, and extremely large positive values (depths >3.5 m). Given this near-normal distribution of snow depth, as well previously observed tendencies of spatial VWC to follow a normal distribution [*Grant et al.*, 2004; *Famiglietti et al.*, 1998; *Western et al.*, 2002], a two-sample t test, and two-sample f test [*Wackerly et al.*, 2008], were carried out at a 5% significance level ($\alpha = 0.05$) to assess the equality of the means and standard deviations between the surveys and network readings. With the exception of the September soil moisture study, these test confirmed null hypothesis H_0 (namely, the equality of the mean and standard deviation between survey and network data). The difference between the September soil moisture survey and network data was deemed statistically significant, with attained significance values (p values) of $p = 0.046$ and $p < 0.0001$ for the mean, and standard deviations tests, respectively. A nonparametric Wilcoxon rank sum test [*Wackerly et al.*, 2008] was also conducted, yielding $p = 0.0625$ for the comparison of the September data sets.

[44] Figure 13 also draws a distinction between those portions of the lidar data that fell below and above the respective minimum and maximum measurements captured by the network. These extreme readings, although not captured fully by the sensors nodes, did not have a significant impact on the overall mean. The majority of locations with snow depth values below those captured by the network were located in the northwestern portion of the network (Figure 13). Larger patches with snow depth values above those captured by the network were located in the centrally situated, open meadow (Figure 13). The distribution of physiographic attributes of uninstrumented locations, for which the set of depth

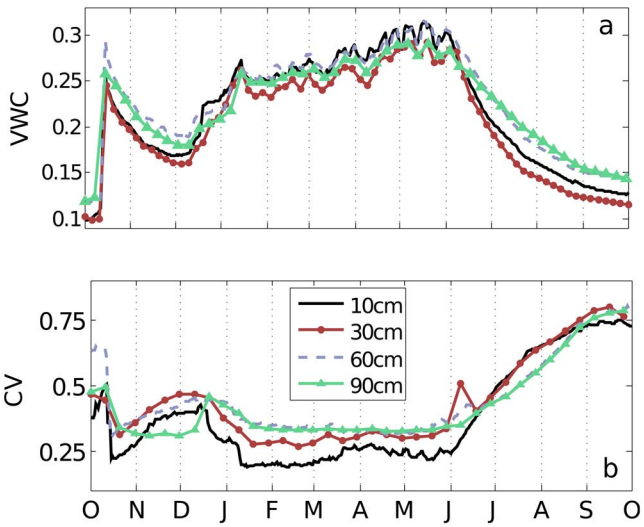

Figure 15. Temporal VWC behavior October 2009 to October 2010. a) Average soil moisture across various solid depths, b) VWC coefficient of variation at various soil depths.

values fell below those captured by the network, did not show signification deviations from those observed on the overall site (data not shown). In the case of both the lidar and synoptic surveys, three particular sensor node locations (Figure 13, yellow stars), situated in a north facing aspect, and across varying canopy cover, reflected measurements very close to the catchment mean (±9 cm).

4.4. Snow Depth Variability

[45] The majority of snow depth readings for water year 2010 (WY2010, starting in October 2009) reached an average peak accumulation of 160 cm in April of 2010, although a subset of nodes experienced this same average peak in the middle of January (Figure 14a). Snowmelt timing showed notable variability, with a 3 week span between first and final melt-out dates at sensor node locations. Nodes located on flat facing aspects generally saw faster melt rates than those on north and south facing aspects, while average accumulation showed little variability across different aspects.

[46] Forest cover was the major explanatory variable of snow depth variability across the catchment. Sensor nodes located under canopy, measured 40 cm less than those located under drip edge, and 80 cm less for open cover (Figure 14b). Under-canopy snow depth showed greater variability, as measured by CV, compared to nodes located in open terrain (Figure 14c). This trend in variability exhibited temporal stability, with under-canopy nodes persistently reflecting relatively higher variability throughout the entire season. The group of nodes located along tree drip edge reflected almost identical variability patterns compared to under-canopy nodes during the snow accumulations seasons. During snowmelt, however, snow depth variability at drip edge nodes began to diverge from that of under-canopy nodes, until matching the variability exhibited by nodes located in open terrain.

4.5. Soil Moisture Variability

[47] At most sensor nodes, peak VWC levels of 0.31 to 0.32 were reached at the beginning of June 2010, coinciding with the melt out of the snowpack (Figure 15a). A subset of nodes experienced peak VWC in the middle of an October 2009 rainfall event. The remainder of VWC fluctuations corresponded with the snowmelt cycle. On average, sensor nodes located on flat aspects experienced VWC 5–10% greater than those situated on north and south facing aspects. The major contribution to this higher VWC was from sensor nodes placed in the flat meadow regions, where catchment meltwater accumulated and some locations experienced VWC of up to 0.60. On average, nodes placed under canopy and in open areas reflected similar VWC behavior, while nodes placed along the drip edge exhibited relative larger VWC (by 0.05).

[48] In general, average variability (CV) of soil moisture increased with decreasing mean VWC following snowmelt (Figure 15b). Shallower soils showed greater VWC fluctuations during the snowmelt season, with VWC fluctuations attenuating with increased soil depth. At a 10 cm depth the relationship between mean soil moisture and the coefficient of variation showed the convex-down pattern (peak at 20% VWC) seen in other studies [*Bogena et al.*, 2010; *Famiglietti et al.*, 1998; *Western et al.*, 2002; *Vereecken et al.*, 2007] (data not shown). The same analysis showed that no clear relationship between mean VWC and CV was apparent for deeper soils.

[49] During snow accumulation and melt, soil moisture variability increased with soil depth, with soils at 10 cm exhibiting lower variability relative to deeper soils (Figure 15b). Following snowmelt, soil moisture variability of the shallow soils exhibited a more pronounced increase in variability. As average soil moisture decreased toward the end of the water year, deeper soils once again exhibited greater variability.

4.6. Geostatistical Analysis

[50] The snow depth values extracted from the March lidar data showed a very well defined experimental variogram, with a range of 30 m and a sill of $\gamma^2 = 0.2\ m^2$ (data not shown). This snow depth variogram was very similar to that seen in *Deems et al.* [2006]. The variogram for the 7 April snow depth survey showed no pronounced support, with a constant sill of $\gamma^2 = 0.2\ m^2$. Variograms were also generated over time for all snow depth readings recorded by the network. While the sill of the sensor node variogram changed over time to reflect depth fluctuations during the season, a support of 30–40 m was evident throughout the analysis. The sill of the variograms generated by the network data also matched that of the lidar and synoptic surveys during the respective analysis periods. The same variogram analysis was carried out for soil moisture surveys and networks readings. Even after detrending for various physiographic parameters, the analysis did not find a clear spatial relationship between lag and VWC variability, such as those seen in previous studies [e.g., *Bogena et al.*, 2010; *Famiglietti et al.*, 1998].

5. Discussion

5.1. Wireless Sensor Network

[51] We define an optimal network deployment as the one that maximizes PDR, while minimizing RSSI (implying greater transmission distances). On average, the need to retransmit data will then be reduced, while spatial coverage of the network will be maximized. Based on this design criterion, Figure 8 shows that this value corresponds approximately to −80 dBm (although there begins to be a significant spread of PDR for values below −70 dBm). This waterfall behavior is a further indicator that a manufacturer-specified RSSI receiver sensitivity threshold dBm should not be employed as a proxy for reliability. In the case of this study, it is apparent than no packets can be received beyond the manufacturers specified threshold of −89 dBm, but PDR begins to exhibit undesirable qualities well before this threshold. As such, the manufacturer specified RSSI threshold thus presents a worst-case performance indicator, rather than serving as a guide for reliable communications. A deployment-specific waterfall plot will however go a long way toward helping to design a reliable WSN.

[52] For our deployment −70 dBm was chosen as a conservative, but reliable, RSSI threshold to account for adverse effects due to unexpected wintertime fluctuations. Given the measured −70 dBm needed for acceptable communications reliability, a design path distance was then extracted from Figure 7. For further reliability, the lower 95% confidence bound, rather than the mean RSSI, was used as the design criteria. For the installation, this resulted in the derivation of a conservative 50 m mote-to-mote spacing. Realistically, however, our redesign could have employed a larger node-to-node spacing (100–120 m), and still performed well, since we did

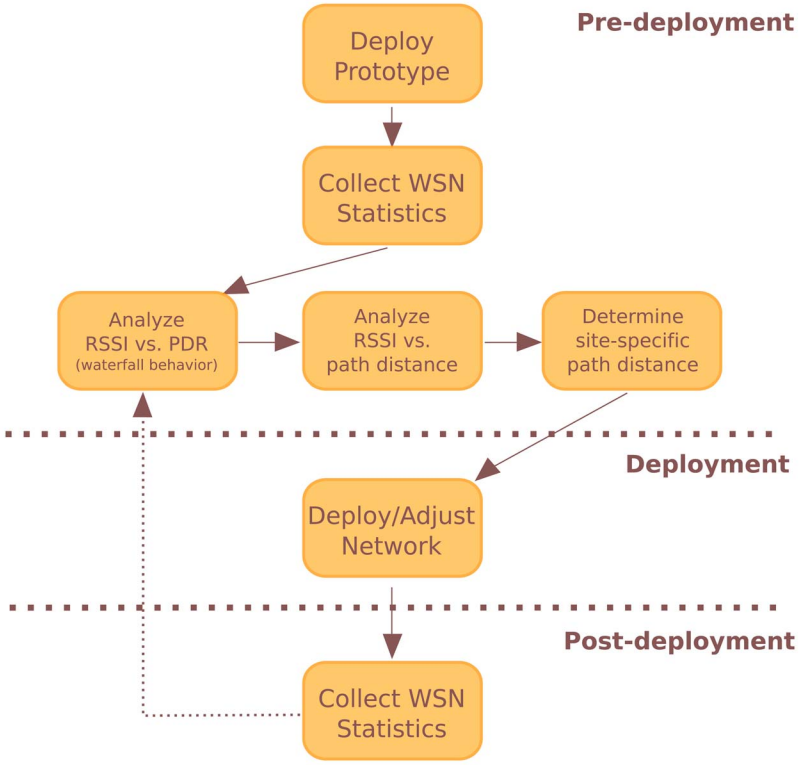

Figure 16. The three phases of a WSN deployment.

observe reliability for such path distances in the final network. Given the expectations of a harsh winter season, and the possibility of nodes getting damaged during heavy snowstorms, we chose a 50 m node-to-node spacing to alleviate any concerns of potential network outages. While our approach is conservative in this regard, we expect that a more temperate, but equally large catchment could be instrumented efficiently with significantly fewer repeater nodes.

[53] It is evident from Table 2 that the mote is the smallest power consumer of the entire sensor node assembly. The choice of snow depth sensor, which consumed a major portion of power at each node, was based on the sensor performance and reliability during a number of previous studies [*Bales et al.*, 2011]. A lower-powered ultrasonic sensor alternative (such as the one in *Varhola et al.* [2010]), could have reduced battery size and solar panel requirements, in which case radio power consumption would begin to play a larger role in overall energy efficiency.

[54] The current availability of power at each sensor node would have made it possible to employ higher-powered radios and thus reduce the number repeater nodes. Given the radio propagation characteristics described previously however, increasing transmission power significantly affects energy consumption, but does not proportionally increase transmission distance [*Friis*, 1971; *Kraus*, 1988]. It can be shown that in many cases, the use of lower-powered radios and efficient repeater nodes consumes overall less power than a system with higher-powered radios but fewer repeaters [*Karl and Willig*, 2005]. This becomes a major motivating factor when considering the need to power the entire wireless network on batteries in remote locations with limited access. In our case, the low cost of repeater nodes, along with their long battery life (potentially 5 years on two AA batteries) and low maintenance continues to motivate our use of the present WSN system. Such low power use and reliability is a particular benefit of the TSMP protocol, with its tight time synchronization and extremely low duty cycle.

[55] We propose a three-step design procedure to optimize a WSN deployment (Figure 16). A WSN deployment can be separated into predeployment, deployment, and postdeployment phases, which, when carried out properly, will ensure robust and reliable network communications while maximizing battery lifetime and transmission distances (and thus reducing the number of required motes).

[56] First, in the predeployment phase, a prototype network (or a subset of the actual network) should be deployed a priori to gauge the actual performance of the wireless hardware under operating conditions. The predeployment analysis should be carried out in environments similar to those of, or preferably at, the actual deployment site, with an attempt to cover a range of terrain parameters. Networks statistics, specifically RSSI and PDR, should be collected for several days, or longer, to capture possible fluctuations in performance. This will place manufacturer specified performance thresholds into context and will permit site-specific network behavior to be evaluated prior to a full-scale deployment. A waterfall plot of the effects of RSSI on PDR (such as the one in Figure 8) should be constructed to extract the site-specific RSSI threshold. The primary design objective entails maintaining stable network links (high PDR values) and ensuring robust network performance. This will prevent network outages and collapse due to the inability of motes to communicate. While maximizing network-wide PDR will reduce retransmissions, and thus also prolong battery life,

there is a monetary and labor trade-off associated with placing many repeater nodes. A PDR of 100% is thus not desirable, and may, in fact, be physically unattainable. Calculations should be conducted to evaluate the effect of average PDR on site-specific battery resources, but in most cases a PDR value of 85–90% provides a realistic performance goal. Such an analysis will maximize node-to-node spacing, while reducing drain on battery resources, and will facilitate robust and reliable network links. It is critical to develop a statistically meaningful RSSI threshold from the PDR behavior to account for possible fluctuations in performance. This threshold can then be used to determine transmission distances (in this case from Figure 7), and will provide a reliable estimate of the number of nodes that will be required to cover the sensing region.

[57] Second, the deployment phase of the final network (placement of sensing nodes, repeater nodes, or star layout) should be carried out based on the previous analysis of network statistics, keeping in mind that these statistics provide only a bound on performance behavior. Signal attenuation and multipath propagation characteristics may adversely affect specific network links. Brief field checks during the actual placement of nodes should be made to ensure that each network path meets the desired RSSI threshold. Often, simply moving nodes by a few meters will establish a more robust link.

[58] Third, in the postdeployment phase, collection of network statistics should be continued as long as necessary to evaluate the in situ performance of the network and to capture possible fluctuations in connectivity. Depending on the observed behavior, these statistics should be further analyzed, and adjustments to the network can be made to achieve a desired performance, by adding, removing, or relocating WSN nodes.

[59] In our case, the data obtained through the analysis of the network prototype was used to gauge the future behavior and provided a set of valuable thresholds upon which to redesign the network. Analysis of such results would have saved a significant amount of time if conducted prior to the deployment of the network. A network design procedure using the above steps will, in most cases, regardless of hardware choice or manufacturer, ensure that WSN performance will meet the demands of an environmental monitoring application, by maximizing path reliability, battery life, and spatial coverage.

[60] While the outlined methods apply to a broad range of available WSN platforms, initial hardware selection should still be strongly guided by built-in network features. The choice of WSN hardware for this deployment was based on the ability of the TSMP protocol to facilitate long battery life, as well as the ability to channel hop and to set up and maintain an adaptive self-healing, multihop mesh network. Regardless of its major benefits, the complexity of this protocol has prevented many manufacturers of WSN hardware from its implementation. There is a significant cost if the direct user is required to design and implement low-level control of the WSN hardware, as well as the complex algorithms necessary for efficient channel hopping and mesh topologies. While lower frequencies (e.g., 900 MHz) can also be used for WSN operations, and may increase transmission distance, availability of these products is trending downward due to regulations in Europe and Asia. Transmission distances can be improved by using high-gain antennas to replace the more traditional mote whip antennas. Close attention to details, such as maintaining sufficient battery voltage at each mote, will additionally help to avoid network blackouts in winter. As most battery chemistries are adversely affected by colder weather, battery specifications should be checked to ensure the minimum amount of current required by the mote can at all times be drawn from the battery, regardless of external temperature.

5.2. Snow Depth and Soil Moisture Variability

[61] This study further confirms the importance of canopy cover as a major explanatory variable of catchment-scale snow depth distribution. More so, it validates the claim that snow depth variability is highest under canopy [*Jost et al.*, 2007]. While those authors investigated the influence of forest cover on snow distribution during a number of surveys, analysis of the spatiotemporally dense data obtained during our study shows that there is a clear temporal stability in this canopy-dependent variability: under-canopy snow depth variability was persistently higher than that of open sites throughout WY2010.

[62] Due to effects of partial canopy cover, sensor nodes located at drip edges of trees showed relatively high snow depth variability during the accumulation season, similar to that of under-canopy nodes. These nodes likely experienced lower long-wave radiation than under-canopy nodes, and but were exposed to higher short-wave radiation in the spring. This further validates the claim by *Jost et al.* [2007] that it is important to consider detailed forest inventory, rather than the binary variable of forest cover, to derive better estimate of snow cover variability.

[63] Our findings on the effect of soil depth on VWC variability are contrary to those of *Bogena et al.* [2010] but agree with *Grant et al.* [2004], who noted an increase in variability at deeper soil depths in a comparably sized mountain catchment. Similar to *Grant et al.* [2004], we attribute this effect to increased heterogeneity of soil properties at greater depths. We also share agreement with *Grant et al.* [2004] on the lack of a correlation between mean VWC and variability (CV), except for near surface measurements. This agreement suggests that there are unique characteristics of VWC variability in mountain catchments that do not follow common findings in a number of other studies [*Famiglietti et al.*, 1998; *Western et al.*, 2002; *Bogena et al.*, 2010].

5.3. Network Measurement Validation and Sampling Design

[64] The ability of the WSN to capture catchment-wide snow depth mean and variability has been confirmed through statistical and qualitative comparisons with the data obtained by the lidar and synoptic surveys. Given this agreement, it is reasonable to suggest that a stratified placement strategy based on evenly instrumenting major physiographic parameters performs well with regard to characterizing the distribution of catchment-wide snow depth at the km^2 scale. Some discrepancies between the snow depth data sets can be attributed to general sensor calibration error. Reflection due to canopy cover may also have introduced noise into the lidar data set.

[65] The approximate 30–40 m support of the snow depth variogram resulting from the geostatistical analysis of both lidar and network data explains why snow depth surveys did not yield distinct variograms. The 125 m spacing between survey locations did not capture smaller-scale variability. If similar length variogram support is validated through future plot-scale surveys, the resulting finding will underscore sampling design: to optimize placement of snow depth sensors, a stratified sampling strategy should be used to cover the range of physiographic parameters on the site, but nodes should not be placed within a variogram range (in this case 30 m) of each other since values within this range can be confidently estimated through geostatisitcal methods (e.g., kriging).

[66] Given the near-normal distribution of snow depth exhibited in the lidar data set (Figure 13), an undersampling of the catchment would not likely capture the extreme values of snow depth. Although the mean and variance estimates were not significantly affected, an example of such undersampling is given by WSN measurements on 22 March, which did not capture the relatively low values in the northwestern region of the catchment, and relatively high values in some of the open meadow regions (dark and light locations in Figure 13). Future placement of a set of sensor nodes in these areas is expected to minimize this bias in coming studies. The nature of WSN technology will permit for the seamless integration of these sensing locations into the existing network. Application of nonlinear classification techniques [*Balk and Elder*, 2000; *Molotch et al.*, 2005] could also reveal if the uninstrumented regions can be more accurately predicted from the instrumented subset of the catchment.

[67] The existence of three sensor node locations (Figure 13, yellow stars) that consistently reflected snow depth mean suggests that it may be possible to identify key measurement locations which capture mean snow depth across the catchment. This notion has been addressed in previous studies [*Molotch and Bales*, 2005], but analysis of multiyear data is required to validate this claim. These points are not associated with any particular physiographic features that could explain this behavior, suggesting that specific spatial coordinates, rather than physiographic attributes, could also serve as indicators of the overall catchment mean.

[68] The discrepancies between the distributions of soil moisture for the synoptic survey and network data were likely influenced by effects of spatial scaling. If the network readings represent the catchment wide VWC distribution, then VWC variability increases over time as the soil begin to dry out after snowmelt. This increase in variability may not have been captured by the 125 m spacing of the synoptic survey. This is particularly true in the case of the September VWC study, in which the network captured high VWC values in meadow regions, thus shifting the estimate of the mean, and increasing overall variability. The layout of the synoptic survey may have undersampled the wet meadow regions, while the spacing between survey locations may have missed the short-scale variations in VWC. Sampling error could also have been introduced by the handheld GPS units used in the study.

[69] Although discrepancies exist between the VWC values captured by the network and synoptic surveys, results suggest that a strategically placed sensor network can effectively characterize the distribution of catchment-wide soil moisture at the km^2 scale. This follows in agreement with *Grant et al.* [2004], who noted that catchment-wide soil moisture could effectively be characterized by few samples. As *Western et al.* [2002] noted, however, it may be of more interest to understand the detailed spatial arrangement of VWC, and effects of physiographic parameters on soil moisture. Such a detailed spatiotemporal analysis [*Famiglietti et al.*, 1998; *Williams et al.*, 2009; *Bogena et al.*, 2010] requires a more spatially dense synoptic data collection.

6. Conclusions

[70] When compared to synoptic surveys and dense lidar data, a sensor-placement strategy based on coverage of physiographic parameters can effectively capture the mean and variability of snow depth across a catchment. Snow depth was also shown to vary significantly based on canopy cover. This variability exhibited temporal stability when comparing under-canopy and open terrain measurements. VWC variability increased significantly following snowmelt, making it difficult to gage sampling design given the density of the synoptic survey VWC data. While the network appeared to capture this increase in variability in the springtime, more detailed plot-scale surveys will be carried out in the future to validate this behavior. A weighted sampling approach, based on the relevance of physiographic parameters and physically based soil moisture, and snowmelt dynamics, may be more suitable for characterizing the VWC behavior at the km^2 scale.

[71] Although WSN technology is continuously improving, no off-the-shelf solution exists for the harsh conditions experienced during most environmental monitoring campaigns. Additionally, few detailed findings are available in previous WSN studies to make conclusive statements regarding their observed performance. Results gathered from the 57-node WSN mesh described in this paper partially fill that gap, by demonstrating a cost-effective means by which to instrument a large, and remote area in complex terrain. Low-power and reliable performance can be achieved by proper evaluation of hardware behavior in the specific field conditions. This deployment successfully covered a 1.5 km transect with a conservative 50 m node-to-node distances, and continues to reliably transmit data from more than 300 sensors every 15 min.

[72] The sheer scale of future monitoring campaigns will demand many network nodes, making it impractical to optimize every single link. In situ network behavior must be quantified to derive average indicators of performance. Gathered over a span of several days, PDR and RSSI should be sufficient to estimate operational path behavior. It is expected that these network characteristics will vary based on site-specific terrain. Unless obvious physical obstacles exist (e.g., large rock outcroppings or metal surfaces blocking a path), the average maximum transmission distance extracted from such an analysis should be sufficient to inform network design.

[73] An open mindset to current limitations of the hardware, and monitoring of network statistics lead to an iterative deployment approach, which can be split into three distinct phases. Since maintaining reliable network performance is the most important design imperative, trading transmission distance for a robust, hardened network is the proper decision. More repeater nodes can be added to improve connectivity and increase connection redundancy, but only collection and

analysis of network statistics can shed light on actual causes of network failure, and lead to rational strategies for improving performance. Using this approach, the network presented in this study experienced significant boosts in performance, and no further collapses.

[74] The implementation of the above deployment strategies should lead to successful WSN deployments of up to 100 nodes, and spanning 1–2 km^2. Environmental monitoring deployments of networks beyond this size should use multiple network managers, each responsible for networks of up to 100 motes. This will reduce the likelihood of large-scale network outages caused by bottleneck effects, while simplifying the identification and management of network behavior. Such architecture permits for manageable approach to scaling, when considering the instrumentation of large areas such as entire basins, or mountain ranges. The network described in this paper is a prototype for monitoring such large areas, and future work will investigate the feasibility and methods of scaling this deployment strategy to cover significantly larger areas. Using these heuristics, deployment time can be significantly reduced, thus allowing more resources to be devoted to the actual scientific program.

[75] **Acknowledgments.** This research was supported by the National Science Foundation, through the Southern Sierra Critical Zone Observatory (EAR-0725097) and a Major Research Instrumentation grant (EAR-0619947). We also acknowledge the cooperation of Carolyn Hunsaker and colleagues at the U.S. Forest Service, Pacific Southwest Research Station, as well as Jan Hopmans, Peter Hartsough, Ryan Lucas, Armen Malazian, and Thomas Watteyne.

References

Al Basset Almamou, A., R. Wrede, P. Kumar, H. Labiod, and J. Schiller (2009), Performance evaluation of routing protocols in a real-world WSN, in *GIIS'09: Proceedings of the Second international conference on Global Information Infrastructure Symposium*, pp. 1–5, IEEE Press, Piscataway, N. J.

Bales, R. C., N. P. Molotch, T. H. Painter, M. D. Dettinger, R. Rice, and J. Dozier (2006), Mountain hydrology of the western United States, *Water Resour. Res.*, *42*, W08432, doi:10.1029/2005WR004387.

Bales, R. C., J. Hopmans, A. O'Green, M. Meadows, P. Hartsough, P. Kirchner, C. Hunsaker, and D. Neaudette (2011), Soil moisture response to snowmelt and rainfall in a Sierra Nevada mixed-conifer forest, *Vadose Zone J.*, *10*, 786–799, doi:10.2136/vzj2011.0001.

Balk, B., and K. Elder (2000), Combining binary decision tree and geostatistical methods to estimate snow distribution in a mountain watershed, *Water Resour. Res.*, *36*(1), 13–26, doi:10.1029/1999WR900251.

Bell, G., and C. Federspiel (2009), Demonstration of datacenter automation software and hardware (dash) at the California franchise tax board, report, Calif. Energy Comm., Sacramento.

Bogena, H. R., M. Herbst, J. A. Huisman, U. Rosenbaum, A. Weuthen, and H. Vereecken (2010), Potential of wireless sensor networks for measuring soil water content variability, *Vadose Zone J.*, *9*, 1002–1013.

Christensen, L., C. L. Tague, and J. S. Baron (2008), Spatial patterns of simulated transpiration response to climate variability in a snow dominated mountain ecosystem, *Hydrol. Processes*, *22*(18), 3576–3588, doi:10.1002/hyp.6961.

Culler, D., et al. (2001), 29 Palms Fixed/Mobile Experiment: Tracking vehicles with a UAV-delivered sensor network, technical report, Univ. of Calif., Berkeley.

Deems, J. S., S. R. Fassnacht, and K. J. Elder (2006), Fractal distribution of snow depth from lidar data, *J. Hydrometeorol.*, *7*, 285–297, doi:10.1175/JHM487.1.

Dust Networks (2006), Technical overview of Time Synchronized Mesh Protocol (TSMP), report, Hayward, Calif.

Etzel, B., and H. Braun (2005), High-performance wireless internet connection to Mount Laguna Observatory, *Bull. Am. Astron. Soc.*, *32*, 1428.

Famiglietti, J. S., J. W. Rudnicki, and M. Rodell (1998), Variability in surface moisture content along a transect: Rattlesnake Hill, Texas, *J. Hydrol.*, *210*, 259–281, doi:10.1016/S0022-1694(98)00187-5.

Faria, D. A., J. W. Pomeroy, and R. L. H. Essery (2000), Effect of covariance between ablation and snow water equivalent on depletion of snow-covered area in a forest, *Hydrol. Processes*, *14*(15), 2683–2695, doi:10.1002/1099-1085(20001030)14:15<2683::AID-HYP86>3.0.CO;2-N.

Friis, H. (1946), A note on a simple transmission formula, *Proc. IRE*, *34*, 254–256, doi:10.1109/JRPROC.1946.234568.

Friis, H. (1971), Introduction to radio and radio antennas, *IEEE Spectrum*, *8*(4), 55–61.

Grant, L., M. Seyfried, and J. McNamara (2004), Spatial variation and temporal stability of soil water in a snow-dominated, mountain catchment, *Hydrol. Processes*, *18*, 3493–3511, doi:10.1002/hyp.5798.

Guo, Q., W. Li, H. Yu, and O. Alvarez (2010), Effects of topographic variability and lidar sampling density on several DEM interpolation methods, *Photogramm. Eng. Remote Sens.*, *76*(6), 701–712.

Hart, K., and K. Martinez (2006), Environmental sensor networks: A revolution in the Earth system science?, *Earth Sci. Rev.*, *78*(3–4), 177–191, doi:10.1016/j.earscirev.2006.05.001.

Hasler, A., I. Talzi, J. Beutel, C. Tschudin, and S. Gruber (2008), Wireless sensor networks in permafrost research—Concept, requirements, implementation and challenges, paper presented at the 9th International Conference on Permafrost, Univ. of Alaska Fairbanks, Fairbanks.

Ingelrest, F., G. Barrenetxea, G. Schaefer, M. Vetterli, O. Couach, and M. Parlange (2010), SensorScope: Application-specific sensor network for environmental monitoring, *ACM Trans. Sensor Networks*, *6*(2), Article 17, doi:10.1145/1689239.1689247.

Institute of Electric and Electronics Engineers (IEEE) (2009), Institute of Electric and Electronics Engineers Standard for Information technology —Telecommunications and information exchange between systems—Local and metropolitan area networks—Specific requirements part 15.4: Wireless medium access control (MAC) and physical layer (PHY) specifications for low rate wireless personal area networks (LR-WPANs), *Tech. Stand. IEEE802.15.4–2009*, IEEE Stand. Assoc., Piscataway, N. J.

International Society of Automation (ISA) (2009), Wireless systems for industrial automation: Process control and related applications, *Tech. Stand. ISA-100.11a-2009*, Triangle Park, N. C.

Jost, G., M. Wirler, D. R. Gluns, and Y. Alila (2007), The influence of forest and topography on snow accumulation and melt at the watershed-scale, *J. Hydrol.*, *347*, 101–115, doi:10.1016/j.jhydrol.2007.09.006.

Karl, H., and A. Willig (2005), *Protocols and Architectures for Wireless Sensor Networks*, John Wiley, Hoboken, N. J., doi:10.1002/0470095121.

Kerkez, B., T. Watteyne, M. Magliocco, S. Glaser, and K. Pister (2009), Feasibility analysis of controller design for adaptive channel hopping, paper presented at First International Workshop on Performance Methodologies and Tools for Wireless Sensor Networks (WSNPerf), Assoc. for Comput. Mach., Pisa, Italy.

Kim, S., S. Pakzad, D. Culler, J. Demmel, G. Fenves, S. Glaser, and M. Turon (2007), Health monitoring of civil infrastructures using wireless sensor networks, in *Proceedings of the 6th International Conference on Information Processing in Sensor Networks*, pp. 254–263, Assoc. for Comput. Mach., New York.

Kraus, J. (1988), *Anetnnas*, McGraw-Hill, New York.

Levia, D., D. Carlyle-Moses, and T. Tanaka (Eds.) (2011), *Forest Hydrology and Biogeochemistry*, Springer, Dordrecht, Netherlands, doi:10.1007/978-94-007-1363-5.

Mainwaring, A., D. Culler, J. Polastre, R. Szewczyk, and J. Anderson (2002), Wireless sensor networks for habitat monitoring, in *Proceedings of the First ACM International Workshop on Wireless Sensor Networks and Applications*, pp. 88–97, ACM Press, New York.

Molotch, N. P., and R. C. Bales (2005), Scaling snow observations from the point to the grid element: Implications for observation network design, *Water Resour. Res.*, *41*, W11421, doi:10.1029/2005WR004229.

Molotch, N. P., M. T. Colee, R. C. Bales, and J. Dozier (2005), Estimating the spatial distribution of snow water equivalent in an alpine basin using binary regression tree models: The impact of digital elevation data and independent variable selection, *Hydrol. Processes*, *19*, 1459–1479, doi:10.1002/hyp.5586.

Musselman, K. N., N. P. Molotch, and P. D. Brooks (2008), Effects of vegetation on snow accumulation and ablation in a mid-latitude sub-alpine forest, *Hydrol. Processes*, *22*(15), 2767–2776, doi:10.1002/hyp.7050.

Oestges, C., M. Villacieros, and D. Vanhoenacker-Janvier (2009), Radio channel characterization for moderate antenna heights in forest areas, *IEEE Trans. Vehicular Technol.*, *58*(8), 4031–4035, doi:10.1109/TVT.2009.2024947.

Pister, K. S. J., and L. Doherty (2008), TSMP: Time synchronized mesh protocol, in *Parallel and Distributed Computing Systems*, edited by T. F. Gonzalez, 475 pp., ACTA Press, Calgary, Canada.

Porter, J., et al. (2005), Wireless sensor networks for ecology, *BioScience*, *55*(7), 561–572, doi:10.1641/0006-3568(2005)055[0561:WSNFE]2.0.CO;2.

Ramanathan, N., T. Harmon, L. Balzano, D. Estrin, D. Hansen, J. Jay, W. Kaiser, and G. Sukhatme (2006), Designing wireless sensor networks as a shared resource for sustainable development, in *ICTD '06: International Conference on Information and Communication Technologies and Development*, pp. 256–265, IEEE Press, Piscataway, N. J., doi:10.1109/ICTD.2006.301863.

Rice, R., and R. C. Bales (2010), Embedded-sensor network design for snow cover measurements around snow pillow and snow course sites in the Sierra Nevada of California, *Water Resour. Res.*, *46*, W03537, doi:10.1029/2008WR007318.

Rice, J., and B. Spencer (2008), Structural health monitoring sensor development for the imote2 platform, paper presented at SPIE Smart Structures Conference/NDE, Int. Soc. for Opt. and Photonics, San Jose, Calif.

Song, J., S. Han, A. Mok, D. Chen, M. Lucas, M. Nixon, and W. Pratt (2008), Wirelesshart: Applying wireless technology in real time industrial process control, in *RTAS '08: Proceedings of the 2008 IEEE Real-Time and Embedded Technology and Applications Symposium*, pp. 377–386, IEEE Press, Piscataway, N. J.

Szewczyk, R., E. Osterweil, J. Polastre, M. Hamilton, A. Mainwaring, and D. Estrin (2004), Habitat monitoring with sensor networks, *Commun. ACM*, *47*, 34–40, doi:10.1145/990680.990704.

Tanenbaum, S. (2003), *Computer Networks*, 4th ed., Prentice Hall, Upper Saddle River, N. J.

Trubilowicz, J., K. Cai, and M. Weiler (2009), Viability of motes for hydrological measurement, *Water Resour. Res.*, *45*, W00D22, doi:10.1029/2008WR007046.

Varhola, A., J. Wawerla, M. Weiler, N. C. Coops, D. Bewley, and Y. Alila (2010), A new low-cost, stand-alone sensor system for snow monitoring, *J. Atmos. Oceanic Technol.*, *27*, 1973–1978, doi:10.1175/2010JTECHA1508.1.

Vereecken, H., T. Kamai, T. Harter, R. Kasteel, J. Hopmans, and J. Vanderborght (2007), Explaining soil moisture variability as a function of mean soil moisture: A stochastic unsaturated flow perspective, *Geophys. Res. Lett.*, *34*, L22402, doi:10.1029/2007GL031813.

Wackerly, D., W. Mendenhall, and R. Scheaffer (2008), *Mathematical Statistics*, 3rd ed., Thomson Brooks/Cole, Belmont, Calif.

Watteyne, T., A. Mehta, and K. Pister (2009), Reliability through frequency diversity: Why channel hopping makes sense, in *PE-WASUN '09: Proceedings of the 6th ACM Symposium on Performance Evaluation of Wireless ad hoc, Sensor, and Ubiquitous Networks*, pp. 116–123, Assoc. for Comput. Mach., New York.

Watteyne, T., S. Lanzisera, A. Mehta, and K. Pister (2010), Mitigating multipath fading through channel hopping in wireless sensor networks, in *2010 IEEE International Conference on Communications (ICC)*, 5 pp., IEEE Press, Piscataway, N. J., doi:10.1109/ICC.2010.5502548.

Watteyne, T., X. Vilajosana, B. Kerkez, F. Chraim, K. Weekly, W. Qin, S. D. Glaser, and K. S. J. Pister (2012), OpenWSN: A standards-based low-power wireless development environment, *Trans. Emerging Telecommun. Technol.*, *23*, 480–493.

Western, A. W., R. B. Grayson, and G. Bloschl (2002), Scaling of soil moisture: A hydrologic perspective, *Annu. Rev. Earth Planet. Sci.*, *30*, 149–180, doi:10.1146/annurev.earth.30.091201.140434.

Williams, C. J., J. P. McNamara, and D. G. Chandler (2009), Controls on the temporal and spatial variability of soil moisture in a mountainous landscape: The signature of snow and complex terrain, *Hydrol. Earth Syst. Sci.*, *13*(7), 1325–1336, doi:10.5194/hess-13-1325-2009.